Lab on a Chip

Devices and applications at the micro- and nanoscale

rsc.li/loc

ROYAL SOCIETY
OF **CHEMISTRY**
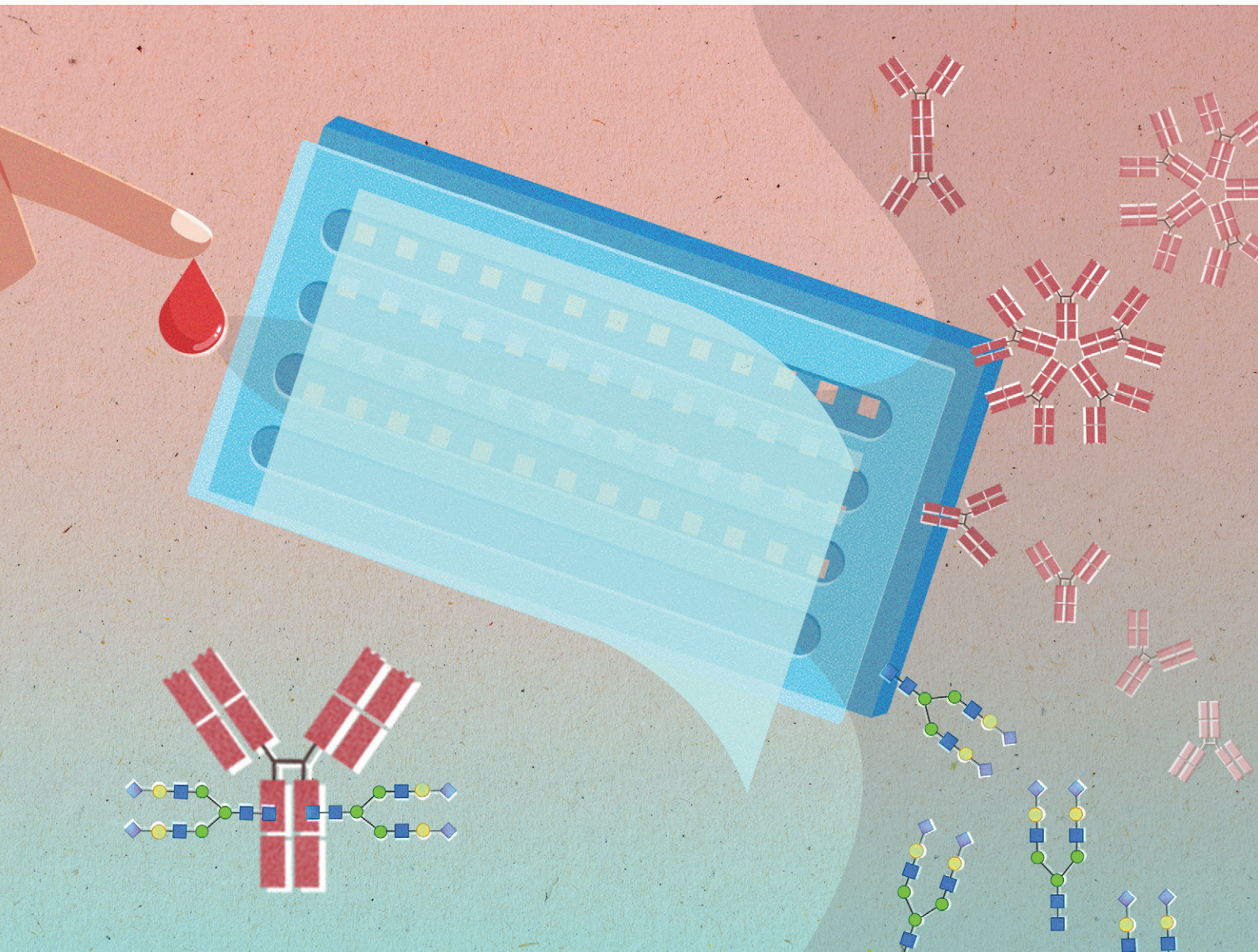
PAPER
Aniruddh Sarkar *et al.*
Sample-sparing multiplexed antibody Fc biomarker discovery
using a reconfigurable integrated microfluidic platform

Check for updates

Sample-sparing multiplexed antibody Fc biomarker discovery using a reconfigurable integrated microfluidic platform†

Hanhao Zhang,[a] Divya Bhakta,[a] Anushka Saha,[a] Sai Preetham Peddireddy,[a] Shumin Bao,[b] Lei Li, [iD][b] Sukwan Handali,[c] W. Evan Secor,[c] Lucia A. O. Fraga,[d] Jessica K. Fairley[e] and Aniruddh Sarkar [iD] *[a]

Control of endemic infectious diseases is often impeded by the lack of sensitive and specific yet easy-to-obtain biomarkers. Antibody fragment crystallizable (Fc) regions, such as Fc glycosylation, which are modulated in a pathogen-specific and disease-state-specific manner have emerged as potential such biomarkers. However current methods to perform large-scale antigen-specific antibody Fc feature screening for biomarker discovery often require too much sample volume, cost and expertise to be realistically realizable in many disease contexts. Here we present a simple, flexible and reconfigurable microfluidic device, made using rapid prototyping techniques, that can perform highly multiplexed and high-throughput biomarker discovery targeting both antibody fragment antigen-binding (Fab) and Fc features including antigen specificity, antibody isotypes, subclasses, *N*-glycosylation and Fc receptor binding. Using integration of an antigen microarray and reconfigurable microfluidics for sample and probe distribution, the device can perform a total of 1400 assays measuring 100 antibody Fab and Fc features per sample from a low sample volume (15 μL). The device demonstrates cleanroom-free simple fabrication and ease of use comparable to standard immunoassay platforms. Performance comparable to existing methods was validated and a biomarker screening for schistosomiasis, a helminth-mediated infection, was performed using clinical samples where antibody subclass-based biomarkers were successfully identified distinguishing current infection from former infection and endemic controls.

Introduction

Control and elimination of endemic infectious diseases are often impeded by the lack of sensitive and specific diagnostic biomarkers that can be measured inexpensively from minimally invasively obtained samples. This includes a range of diseases from those that are considered newly endemic, such as COVID-19,[1] to those that have been around for millennia, such as tuberculosis (TB)[2] or schistosomiasis.[3] These diseases can be caused by a variety

of pathogens including viruses, mycobacteria and helminths.

Direct pathogen detection *via* microscopy or pathogen-derived molecular biomarker-based tests remains the gold standard but is complex and costly or has low sensitivity for many infections. This can be due to low target abundance, complex sample acquisition (*e.g.* sputum for TB) and preparation or varying pathogen burden and sequestration in tissue over its life cycle. Monitoring of host immunity, especially antibodies (Abs), can provide an amplified readout of infection. Abs make up to 20% of protein in blood.[4] Their abundance in blood and other easily accessible samples, along with their inherent ability to bind pathogen-specific antigens, enables easy testing of their presence using inexpensive formats such as lateral flow assays from small sample volumes.

Ab titer-based tests however cannot accurately distinguish current from past infection and thus have low specificity for endemic infections because Abs tend to linger after infection.[5] Abs are composed of two functional domains: fragment antigen-binding (Fab) and fragment crystallizable (Fc) (Fig. 1A). While pathogen-specific binding occurs *via*

[a] Department of Biomedical Engineering, Georgia Institute of Technology, 315 Ferst Dr NW, Atlanta, GA 30332, USA. E-mail: aniruddh.sarkar@bme.gatech.edu
[b] Department of Chemistry and Center for Diagnostics & Therapeutics, Georgia State University, Atlanta, GA, 30303, USA
[c] Division of Parasitic Diseases and Malaria, National Center for Emerging and Zoonotic Infectious Diseases, Centers for Disease Control and Prevention, Atlanta, GA 30333, USA
[d] Federal University of Juiz de Fora, Juiz de Fora, Minas Gerais 36036-900, Brazil
[e] Department of Medicine, Division of Infectious Diseases, Emory University School of Medicine, Atlanta, GA 30307, USA
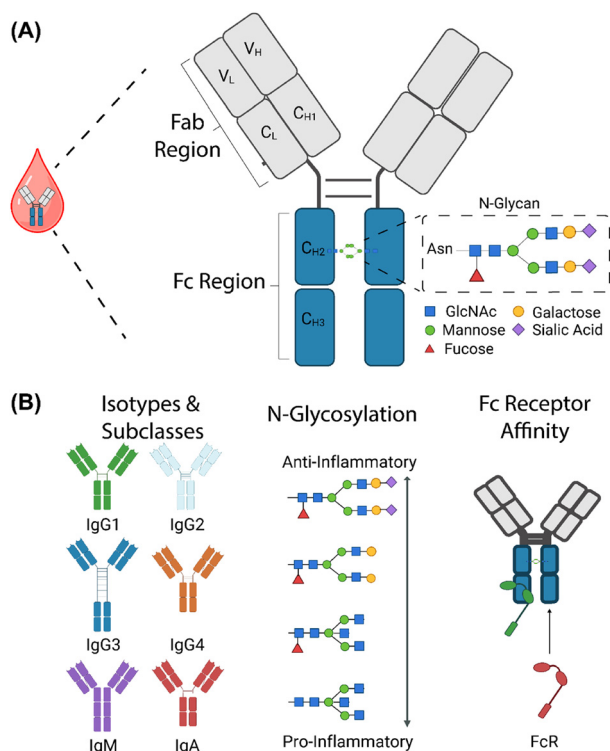† Electronic supplementary information (ESI) available. See DOI: https://doi.org/10.1039/d5lc00042d

Fig. 1 (A) Structure of an antibody with Fab, Fc and *N*-glycans labelled. (B) Antibody Fc features, including isotypes/subclasses (left), *N*-glycosylation (middle) and affinity to Fc receptors on cells (right).

the Fab region, effector functions are directed by the Fc region. This Fc region is rapidly modified during an immune response in two distinct ways: a) distinct isotypes (IgG, IgA, IgM, IgE) or subclasses (IgG1–4, IgA1–2) may be selected (Fig. 1B) or b) differential Fc glycosylation may occur, which is a post-translational modification carried by all human Abs (Fig. 1B). Both these Fc modifications regulate Ab binding to complement and Fc receptors carried by immune cells thus regulating host immune functions including antibody-dependent cellular cytotoxicity, phagocytosis, *etc.*[6,7] Among these two, Ab glycosylation has been shown to shift in a disease-state-specific manner[7] and thus has emerged as a disease-state-specific predictive biomarker. We have recently shown that a comprehensive measurement of Fab and Fc properties of Abs *via* antigen specificity, isotype, subtype, glycosylation and Fc receptor binding measurement, coupled to machine-learning-based analytics (termed together as *Ab-omics*), can be used to predict outcome in severe COVID-19 and disease state in schistosomiasis.[8,9] Others have described Ab glycosylation and Fc-related biomarkers in HIV,[10] dengue,[11] TB,[12] rheumatoid arthritis,[13] colorectal cancer[14] and even aging.[15]

However, despite increasing interest in Ab glycosylation- and Fc-based biomarkers, there is a scarcity of tools for their discovery from low-volume clinical samples. Mass spectrometry (MS)-based methods remain the gold standard for glycomics studies. However, these are cumbersome, expensive and, critically, require prior isolation of antigen-

specific Abs, which demands large volumes of sample (*e.g.* ~0.1–1 mL of blood per antigen specificity). Thus, they need an impractically large sample volume for profiling large numbers of antigen-specific Abs (*e.g.* for a complete immunoproteomic scan of ~4000 antigens of *M. tuberculosis*, it would need ~400–4000 mL of blood per patient). Recently developed glycan-specific probe binding-based methods including lectin-[8,9] and nanobody-based Ab glycoprofiling[11] and multiplexed Ab Fc profiling methods[16,17] offer an opportunity for reducing the sample requirement for Ab Fc biomarker discovery. However, these assays remain too specialized currently compared to standard immunoassays commonplace in clinical research laboratories, such as plate-based enzyme-linked immunosorbent assays (ELISAs). Conversely, traditional ELISAs lack multiplexing ability and would require multiple runs for measuring Fab (antigen) and Fc (probe) combinations adding to labor and sample requirement.

Microfluidics offers an attractive alternative for massively multiplexed immunoassays. Microfluidic devices can test high numbers of samples simultaneously while using only a few microliters from each.[18,19] However, fabrication and use of such devices are still complex, requiring techniques and training not easily accessible to clinical research labs with most interest in biomarker discovery, especially in resource-poor settings, which may however be well-trained in typical immunoassay workflows.

To overcome the above obstacles, in this work, we set out to develop a simple, easy-to-manufacture and easy-to-use microscale device that can be used for highly multiplexed Ab Fab and Fc profiling for biomarker discovery from small volumes of clinical samples. We achieved this *via* the integration of antigen microarrays on glass slides with flexible and reconfigurable microchannels made using widely available rapid prototyping tools. The device and workflow (Fig. 2) are designed to be usable with high tolerance during assembly and operation and with minimal additional training beyond that for a typical multi-channel pipette compatible immunoassay workflow. Here we report the design and development of this chip, which we term as the Microfluidic Multiplexed Antibody-omic Profiling (or μMAP) chip, which performs 1400 Ab Fab and Fc assays simultaneously, establish its performance compared to other methods, and demonstrate its use in characterizing small volumes (15 μL) of clinical samples from schistosomiasis patients to find an active infection-specific biomarker which clearly distinguishes current infection from former infections.

Results and discussion

μMAP device and assay workflow design

We first developed the inexpensive, easy-to-manufacture and easy-to-use μMAP device for highly multiplexed simultaneous measurement of Ab Fab properties, *i.e.* antigen-binding and various Fc properties for each Fab specificity, including Ab
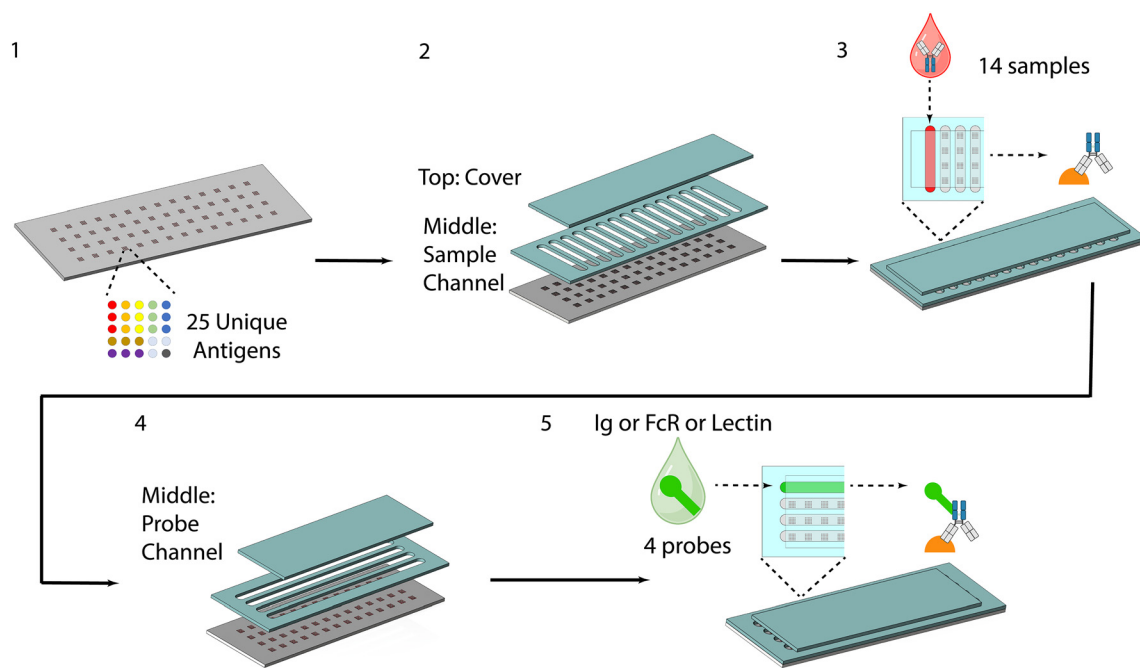
Fig. 2 Schematic of the workflow of the device, including: 1. microarray printing, 2. sample channel attachment, 3. sample addition, incubation and removal, 4. probe channel attachment, 5. probe addition, incubation and removal.

isotypes, subclasses, *N*-glycosylation and affinity to Fc receptors (Fig. 1B). To overcome the drawback of requiring large volumes of samples for antigen-specific Ab isolation when performing LC-MS or the use of separate sample aliquots for ELISA, we integrated protein microarrays and microfluidic channels (Fig. 2). The multiplexing capability of the μMAP chip, due to the 25 capture antigen spots used for each sample/Fc probe combination, significantly reduces sample usage. This can be compared with the requirement for preparing 25 separate portions of the same sample and then isolating, *via* binding and elution steps, each of the antigen-specific antibodies for measuring glycosylation on each of them as is the case when measuring glycosylation on antigen-specific antibodies using LC/MS. The microfluidic channels provide parallelized sample distribution and Fc probe multiplexing ability for completing the binding sandwich assay in a high-throughput and highly multiplexed format. Typically, microfluidic devices which implement sandwich immunoassays use microfluidic valves to redirect fluid flows between assay steps.[20–22] Here, for ease of fabrication and ease of use by non-experts, we use removable channels made from a stack of two thin (0.01″/0.02″) and flexible PDMS sheets instead which can be easily removed and replaced between assay steps reconfiguring the flow paths as needed for the next assay step.

To further simplify the fabrication, we avoid here the conventional process of creating a lithography-based mold and then molding a piece of PDMS. Instead, we formed the enclosed microfluidic channels by simply pressing two pieces of the above thin laser-cut PDMS sheets onto a glass slide. The glass slide serves as the bottom, the middle

PDMS sheet, which has laser-cut channels, serves as the side walls while the top PDMS sheet serves as the cover. The PDMS sheet used is commercially available, as a roll, at a low cost (<\$20 per sq. ft.). The cutting of the channels only requires simple laser cutting using a basic laser cutter available in most rapid prototyping facilities globally.[23] Due to its minimal thickness, the sheet is highly conformable and ensures good sealing when simply pressed against the glass slide. As a result, the fabrication of this microfluidic device does not involve any conventional cleanroom fabrication techniques and can easily be done in a typical wet lab environment. To reduce sample usage by decreasing the height of the channels, 0.01″ thin PDMS was chosen for the middle sample channel layer. After full assembly, less than 15 μL of sample is enough to fill each vertical sample channel and covers four 25-plex antigen array blocks per column, which equals testing against all combinations of 25 capture antigens and 4 Fc probes – thus measuring a total of 100 Fab and Fc properties per sample. This can be compared to the assay volume of a standard microtiter-plate well in a single-plex ELISA, which is ~40 μL per feature measured and would thus add to ~4 mL per sample for the 100 measurements.

The complete μMAP-based assay procedure is shown in Fig. 2. First, the glass slide is spotted with capture antigens in a 5 × 5 array format (see Experimental section for spotting details). 8 different proteins with 3 replicates plus a control are shown in the example array here, yet the type and numbers of antigens are customizable at this stage. Here, each slide has 14 columns and 4 rows of the 5 × 5 antigen array blocks printed. To perform the biomarker discovery experiment, two

layers of PDMS are pressed on the glass slide without irreversible bonding to form channels. Samples are then added into the vertical sample channels using a single-channel or multi-channel pipette. These channels get filled by a combination of capillary action and the gravity head due to the sample drop placed at the channel inlet; thus the assay procedure does not require the use of any additional pumping equipment. After sample incubation, these PDMS layers are removed in PBS without cross contamination. The slide is washed and dried, and another two layers of PDMS are attached and four fluorescently labelled Fc probes are added into the 4 horizontal channels for incubation. After PDMS removal and slide washing, a fluorescent signal from each protein dot can be read. Here we use a standard microarray scanner for this as this offers automation in reading, but a standard fluorescence microscope can also be used for this.

μMAP device prototyping and development

The layout of the microarray-printed slide is illustrated in Fig. 3A. To provide easy yet accurate alignment between chip and removable PDMS channels, clear rectangular alignment marks (Fig. 3B) were created on both the chip

and middle PDMS layer *via* laser engraving. Two additional cross marks (Fig. 3C) were created on the chip to set the coordinates of microarray printing to ensure precise protein placement. An optical image of an example 5 × 5 array after printing is shown in Fig. 3D. Protein spots within the array were found to be highly aligned and had highly repeatable spot size. The middle PDMS layer formed channels for 14 samples (Fig. 3E) and 4 probes (Fig. 3F). Though 0.01″ thick PDMS was chosen for the sample layer to minimize sample volume usage, volume was no longer a restriction when probes were added, as probes were commercially available at high stock concentrations and required dilution before usage. As a result, thicker 0.02″ PDMS was chosen for the probe layer as the increased height enabled less channel resistance when flowing probe solution through the longer probe channels. It also improved device integrity and ease of manipulation. Given this advantage, thick PDMS was chosen for the top layer as well. To attach the middle layer on the chip, a 3D printed alignment block (Fig. S1†) was used to keep the flexible middle layer channels in a straight and equally spaced format (Fig. 3G). A complete assembly after attaching the top layer (Fig. 3H) showed no leakage after injecting dyes into the channels (Fig. 3I).
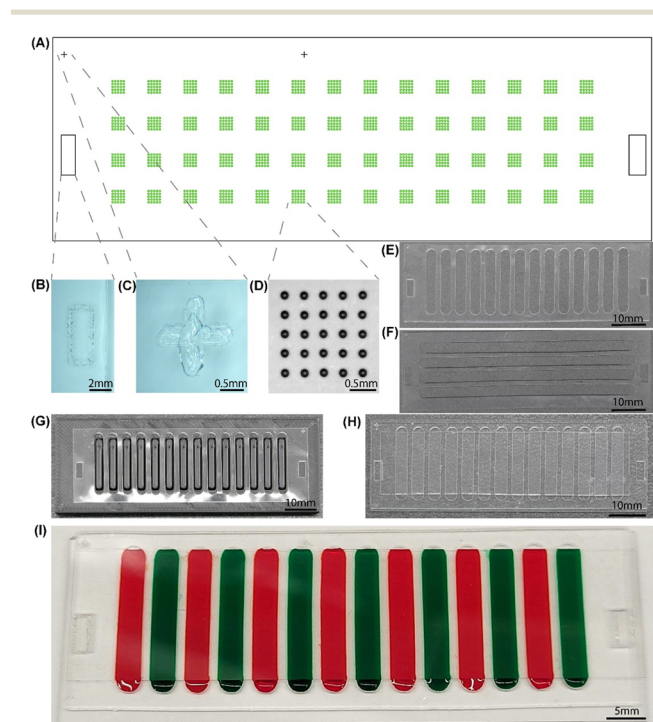

Fig. 3 Physical design of the device. (A) 2D layout of alignment marks and microarrays on the glass slide. (B) Optical image of an alignment mark used by PDMS attachment. (C) Optical image of an alignment mark used by microarray printing. (D) Optical image of a 5 × 5 array after printing. (E) PDMS middle layer for sample. (F) PDMS middle layer for probes. (G) Sample middle layer rectified on 3D printed alignment block. (H) Optical image of the device after full assembly. The sample version was used as the middle layer. (I) Demonstration of the assembled device with colored dye filling the channels as samples.
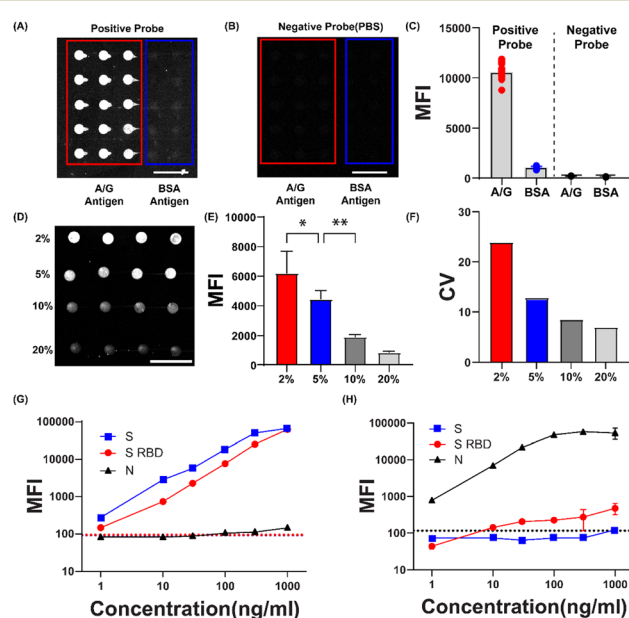

Fig. 4 Performance verification and optimization. (A) Fluorescence image of an array exposed to antibody sample (IgG) and positive probe (anti-IgG-PE). (B) Fluorescence image of an array exposed to antibody sample (IgG) and negative probe (PBS). (C). MFI of arrays in (A and B). N = 15 for A/G and 10 for BSA. (D) Fluorescence image of an array with capture antigens printed in different concentrations of glycerol. (E) MFI of the array in (D). (F) Coefficient of variation of the array in (D). (G) Dilution curves of monoclonal anti-SARS-CoV-2 spike IgG against various antigens. Dotted line represents averages of background plus three times its variation. N = 2. (H) Dilution curves of monoclonal anti-SARS-CoV-2 nucleocapsid IgG against various antigens. Dotted line represents averages of background plus three times its variation. N = 2. Scale bars in (A, B and D) equal 500 μm.

µMAP assay optimization and verification

To verify the operation and usability of the µMAP device, we conducted various performance tests. Specificity of the immunoassay using printed capture antigen spots on chip was verified using comparing signal intensity within an array exposed to a commercially obtained monoclonal Ab sample and a specific probe against it (Fig. 4A). The 3 left-hand columns with positive control antigens (protein A/G) returned high mean fluorescence intensity (MFI) while the 2 right-hand negative control antigens (BSA) returned low MFI, which was barely visible. Specificity of the fluorescent probe in the µMAP assay was verified by comparing MFI between two arrays exposed to positive control probe (anti-IgG-PE, Fig. 4A) and negative probe (BSA, Fig. 4B). On positive control antigens, positive control probe returned high MFI while negative control probe returned low MFI which was barely visible. Combining Fig. 4A and B, we confirmed that only when both positive antigen (protein A/G) and positive probe (anti-IgG-PE) are present will the corresponding spot yield fluorescence (Fig. 4C). Leakage-free operation was also again functionally verified here since positive probes and negative probes were placed in neighboring channels, and no cross-channel contamination was observed after the assay. Stability of the printed protein was verified for up to two months (Fig. S3†).

To ensure good repeatability, we explored methods to improve the morphology of the printed protein dots. Besides optimizing settings of the printer, we added glycerol as it is known as an agent that can stabilize a liquid drop during protein microarray printing.[24] An increase in repeatability of morphology of printed dots was observed by adding more glycerol (Fig. 4D), yet it came at the cost of lower MFI. By considering MFI (Fig. 4E) and variation (Fig. 4F) of the drops, 5% glycerol was chosen as the optimal concentration to achieve a balance. To demonstrate the ability of the device to perform a sandwich binding immunoassay, serial dilutions of monoclonal IgG targeting different antigens were added to different channels of the same chip printed with SARS-CoV-2 antigens. For the channel infused with anti-spike (S) Ab, MFI from both spike and spike RBD (S RBD) protein (which is the receptor binding domain and hence part of the S protein as well) formed a sample dilution-dependent response curve, while MFI from the non-target nucleocapsid (N) protein remained low around background (Fig. 4G), proving the ability to measure the concentration of antibody in buffer quantitatively and specifically. LOD for the above application reached 1 ng mL^{-1} (6.7 pM), while a dynamic range of >3 orders of magnitude were achieved. Note that this is similar sensitivity to that achieved in typical plate-based single-plex ELISAs. However, it represents higher dynamic range (>3 orders of magnitude) than most plate-based ELISAs (2–3 orders of magnitude) while being multiplexable as well. Similarly, for the channel with anti-N Ab as sample, MFI from N protein spots formed a sample dilution-dependent response curve, while the MFIs from S and S RBD proteins in this channel remained low (Fig. 4H), again verifying the specificity of the immunoassay in the µMAP chip. As the two

types of antibodies and probes were all placed in neighboring channels, no cross contamination was again verified. Verification with clinical samples was also performed with serum from a SARS-CoV-2 patient and vaccinated and pre-pandemic healthy individuals. Antigen-specific IgG against 8 antigens were measured using one chip simultaneously. Decreasing MFI of spike-specific antibody when serum dilution increased verified the ability of µMAP to measure antibody titer (Fig. S4†). The measured MFI of IgG against N/S/S RBD between the three groups verified the function and throughput of the µMAP chip (Fig. S5†).

Antibody glycosylation and Fc receptor binding measurement

To address the need for quantifying more Fc features, namely the level of *N*-glycosylation, two fluorescently tagged lectins (*Sambucus nigra* lectin or SNA and *Ricinus communis* agglutinin or RCA) were chosen as the probes targeting glycans (Fig. 5A) to comply with the binding assay format of the µMAP chip. SNA specifically binds α2,6-sialic acid[25] on
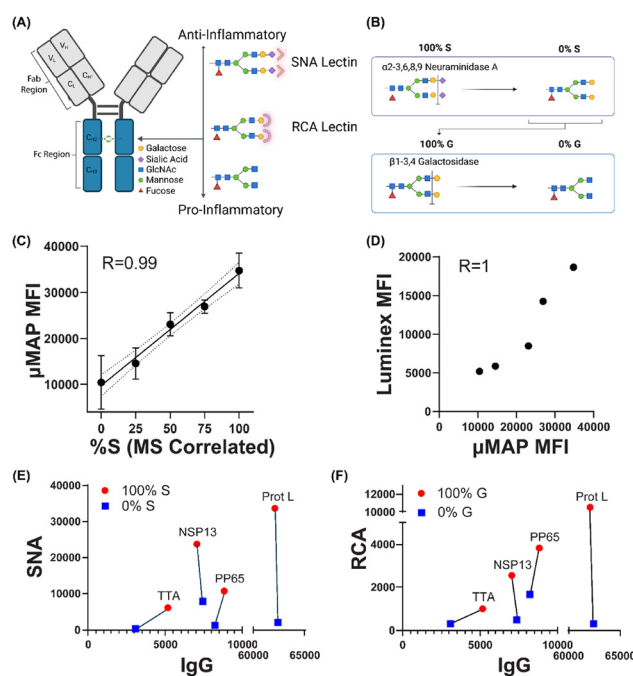

Fig. 5 Design and result of *N*-glycosylation detection on the device. (A) Illustration of the glycan–lectin binding mechanism. PE-labelled SNA specifically binds to sialic acid while PE-labelled RCA specifically binds to galactose. (B) Illustration of serum glycan engineering using enzymes specifically cleaving off sialic acid and galactose. (C) Pearson correlation of measured % sialic acid on antibodies against protein L between the device and LC-MS in engineered samples. *N* = 6. (D) Spearman correlation of measured % sialic acid on antibodies bound to protein L between device and Luminex in engineered samples. (E) MFI of SNA *versus* IgG probe for samples with no sialic acid removal (100% S) and all sialic acid removed (0% S). Data from the same capture antigen are connected by a solid black line. *N* = 3. (F). MFI of RCA *versus* IgG probe for samples with no galactose removal (100% G) and all galactose removed (0% G). Data from the same capture antigen are connected by a solid black line. *N* = 3.

glycans, especially Neu5Acα2,6GalNAc while RCA specifically binds galactose or *N*-acetyl galactosamine motifs,[26] especially terminal type 2 LacNAc. Both these specific glycans are known to change with disease state in several infections.[8,9] Besides specific probes, to validate the performance of the chip, a sample containing antibodies with quantified level of *N*-glycosylation was required. To create such samples, *in vitro* enzymatic glycoengineering of normal human serum containing antibodies was performed. First, sialic acid-specific cleavage was performed using the enzyme α2-3,6,8,9 neuraminidase A (Fig. 5B). After enzymatic digestion, the original human serum samples containing antibodies with native amount of sialic acid (labelled 100% S) were transformed into samples with no sialic acid (labelled 0% S). Similarly, the asialated samples with unmodified galactose on antibody (labelled 100% G) were transformed into those with no galactose (labelled 0% G) *via* enzymatic cleavage using the β1-3,4 galactosidase enzyme (Fig. 5B). As not every glycan on human antibodies has sialic acid, the 100% S was not the actual quantification of sialic acid but was used as a label which represents the level of unmodified sialic acid for ease of understanding. However, the sialylation and galactosylation levels of these samples were verified using a standard LC-MS based glycomics workflow,[27] which closely correlates with the labels. Details on actual percentage of sialic acid for each label can be found in Table S2.†

Using serum samples that underwent the above modifications, 100% S and 0% S samples, and mixtures thereof, were tested on the μMAP chip using protein L as the capture antigen spot, which bind all isotypes and subtypes of antibodies *via* their Fab region. A linear relationship between percentage of sialic acid in samples, measured using LC-MS, and corresponding measured MFI of SNA binding on antibodies on the μMAP chip was observed (Fig. 5C). The linear pattern, repeatability and the high correlation of 0.99 with the gold standard MS indicated that the μMAP chip could accurately quantify the level of sialic acid on antibodies in human serum. One trade-off we observed was that unlike results from LC-MS, the 0% S sample returned an MFI close to that of the 25% S sample. This was likely due to the nature of the lectin probe exhibiting high background binding, and 0% S was out of the dynamic range of this method when used for quantifying glycosylation. Data from the μMAP chip were also highly correlated with data from a bead-based lectin-binding assay (Luminex) with the same set of samples (Fig. 5D). Here, the same issue with measuring 0% S occurred for the bead-based assay, indicating this issue was common to binding assays utilizing this lectin probe and not dependent on the use of the μMAP chip.

Next, we tested if the μMAP chip can simultaneously measure antibody glycosylation of multiple antigen-specific antibodies, which is the key bottleneck in MS-based glycomics that drives high sample usage. Enabled by the high-throughput nature of the chip, sera from healthy individuals containing either unmodified antibodies or asialated/agalactosylated antibodies after *in vitro* enzymatic

glycoengineering of serum as described above were tested against 4 antigens (Protein L, CMV pp65, Tetanus (TTA), and SARS-CoV-2 nsp13) and 2 lectins (SNA, RCA) plus anti-IgG probes simultaneously on one μMAP chip. The results of this are shown in Fig. 5E and F. Each datapoint represents properties of antibodies targeting one specific antigen, with the *X* value representing the titer of antigen-specific IgG and the *Y* value representing the level of glycans as measured *via* lectin binding for that antigen-specific Ab. While protein L is a positive control that binds all Abs, the other three antigens here were chosen because healthy donors are expected to have antibodies against them due to childhood vaccination (tetanus) or common prior infection (CMV, SARS-CoV-2 or other endemic human coronaviruses). For the sialic acid-modified samples, the MFI of IgG remains similar between the two groups while the MFI of SNA decreased significantly for antibodies after sialic acid removal (Fig. 5E). As the slope of the connecting line represents a change in SNA quantity
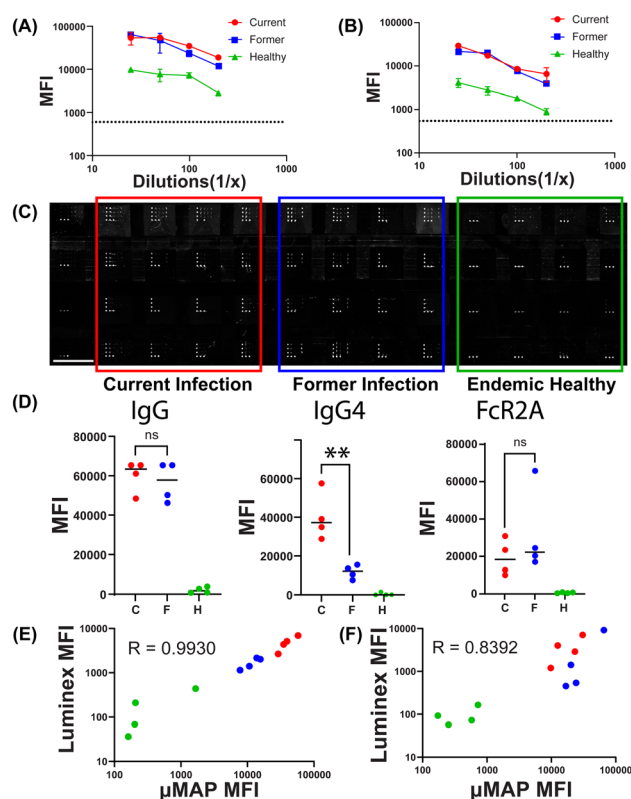

Fig. 6 Device performance on serum samples from persons with current active schistosome infection (red, label C), former infection (blue, label F) or never infected/healthy (green, label H). (A) Dilution curves of SEA-specific antibodies in pooled samples that had affinity with FcR2A. *N* = 3. (B) Dilution curves of SEA-specific antibodies in pooled samples that had affinity with FcR2B. *N* = 3. (C) Fluorescent image of an entire device that was used to perform biomarker discovery on 12 samples and 4 probes for schistosomiasis. Scale bar equals 4 mm. (D) MFI of SEA-specific IgG (left), IgG4 (middle) or affinity with FcR2A (right) in individual samples. *N* = 3. (E) Spearman correlation between device readout and Luminex for SEA-specific IgG4 in individual samples. (F) Spearman correlation between device readout and Luminex for SEA-specific FcrR2A affinity in individual samples.

over change in IgG titer, the close-to-vertical lines in Fig. 6E indicated the difference in SNA–IgG ratio matched the property of the two samples due to sialic acid cleavage and was accurately captured by the µMAP chip, validating its ability to measure the level of Fc N-glycosylation. Tetanus-specific IgG was the only exception, where a small decrease in IgG MFI was also observed after sialic acid removal. We suspect that the antigen-binding Fab region in this case had been affected by the sialic acid removal process. The same validation was observed for agalactosylated samples when tested with RCA binding on the µMAP chip (Fig. 5F). This establishes the key ability of the µMAP chip to perform multiplexed antigen-specific Ab glycoprofiling from small volumes (1000 times lower than for MS) of serum samples.

Clinical biomarker discovery for schistosomiasis

After verifying its performance for multiplexed Ab Fab and Fc profiling, we utilized the µMAP platform to perform biomarker discovery using clinical patient samples for schistosomiasis (Schisto) from persons with *Schistosoma mansoni* infections. This is a helminth-mediated infectious disease that is endemic in many tropical countries and often occurs in low-resource settings.[28] Presence of parasite eggs in stool (Kato Katz test) is what is commonly used to diagnose infection but suffers from low sensitivity in low-prevalence settings. Ab-based tests for schistosome infections are more sensitive, but they are usually unable to distinguish current from former infections because antigen-specific Abs can persist following treatment. To improve the diagnostic value from an Ab-based test, we aimed to identify Ab Fab- and Fc-based biomarkers that differentiate between current active infection, that is, persons seropositive for Ab against schistosome soluble egg antigen (SEA) and had eggs detected in stool samples (SEA+Egg+); former or non-patent infection, that is, individuals seropositive for Ab against SEA but with no eggs detected in stool samples (SEA+Egg−); and endemic healthy controls, that is, persons seronegative for Abs against SEA and egg negative (SEA−Egg−).

We first verified if Ab Fc receptor binding could be quantified in Schisto patient serum samples by measuring the MFI of SEA-specific antibodies that had affinity with FcR2A (Fig. 6A) and FcR2B (Fig. 6B) in pooled serum samples. Clear sample dilution-dependent response curves were formed with trends matching the nature of the samples. The two infection groups had higher MFI compared to endemic healthy controls. Next, we screened 12 individual patient serum samples from the 3 groups (C, F, H) against a set of 5 *S. mansoni* antigens (SEA, SM25, MEG, CD63, Calumenin B), 2 control antigens and 4 probes (IgG, IgG4, FcR2A, FcR2B) on one µMAP chip (Fig. 6C). After 2 h of assay and subsequent data processing (total <3 h), we obtained the MFI readouts from ~1000 antigen–antibody–probe combinations, *i.e.*, coupled Fab and Fc combinations, and used these data to evaluate potential biomarkers. The full Ab dataset is included in Fig. S6–S8.† Analyzing these data, we

found that while SEA-specific IgG was low for endemic controls (SEA−Egg−), it was high in both current (SEA+Egg+) and former infected individuals (SEA+Egg−). Thus SEA-specific IgG alone could not differentiate between current and former infections (Fig. 6D, left), consistent with prior studies. By contrast, SEA-specific IgG4 successfully differentiated current from former infection (Fig. 6D, middle). This suggested that the amount of SEA-specific IgG4, an IgG subclass and an antibody Fc feature, could be a promising biomarker that differentiates different stages of schistosome infection. The MFI of the SEA antibody-IgG4 combination obtained from the µMAP chip yielded a strong correlation of $R = 0.9930$ with that obtained from the bead-based assay readouts (Fig. 6E), further validating the reliability of the µMAP chip when applied on individual patient serum samples. Antibodies specific to other antigens yield less difference when compared between these groups (Fig. S6–S8†). Although the other suspected Fc features tested here (Ab affinity against FcR2A/2B) did not differentiate current active from former infections in these samples (Fig. 6D, right), the MFI from the µMAP chip again yielded a strong correlation with results from bead-based assays (Fig. 6F), indicating that the µMAP chip also had the ability to measure other Ab Fc features in individual serum samples.

Overall, the µMAP chip has several distinct advantages compared to existing solutions for Ab Fc biomarker discovery. By using a highly multiplexed microarray and microfluidic channels, it requires far less sample (100–1000 times lower volume), labor and cost compared to conventional MS and ELISA (Table S1†). This sample volume reduction represents a critical enabling advantage in Ab Fc biomarker discovery for many disease contexts, where potentially large numbers of antigen specificities may have to be screened to find the right set of Ab Fab and Fc features that can act as the most accurate biomarker with high sensitivity and specificity in distinguishing specific infection or disease states.

Compared to other approaches that combine microfluidics and microarrays for Ab detection,[19,29] this work is, to the best of our knowledge, the first to target not only Ab titer but also Ab Fc features including N-glycosylation and Fc receptor binding. The µMAP chip does have some unique trade-offs as well when compared to traditional microfluidics. These are the result of conscious unique design choices made here to make it more appropriate for its target use settings. The assay time (<3 h) and level of manual operations of the µMAP chip are still closer to those of a lab-based ELISA when compared to automated microfluidic approaches.[20,22] While some simple manual operations are still required, the µMAP platform focuses on simplifying and reducing the cost and expertise requirement of device preparation and fabrication: instead of requiring automated valves/pumps/magnetic actuators and controlling electronics, the device only uses thin laser-cut PDMS sheets and a glass slide. The PDMS sheets required for each device are commercially available, can be patterned with cleanroom-free procedures in 2 min, and cost less than $1.5 each, whereas PDMS components in

traditional automated microfluidics require soft lithography, molding and other modifications, taking significant expertise and days to fabricate. In using this platform, though there are additional steps required after sample addition, those steps such as slide washing and thin-film adhesion are commonly within the existing expertise of clinical research laboratories that routinely perform ELISAs. Thus, the μMAP platform may be especially appropriate for use in clinical or public health laboratories in resource-limited regions. The proposed μMAP workflow starts with microarray slides and PDMS sheets which can be batch produced, remain stable under proper storage, then sent to research labs in resource-limited regions that can use local serum samples to perform the assay for biomarker discovery. In such regions where infectious diseases are prevalent, but shipping samples internationally is restricted, it may be reasonable to sacrifice some level of automation in exchange for significantly reducing the cost and the required additional hardware, such as syringe or peristaltic pumps *etc.* and the learning curves associated with device use and maintenance.

We also note that while a microarray scanner is used here, which is not common equipment in resource-limited regions, this is not a critical requirement for the operation of this chip. Various prior works have shown portable or easy-to-fabricate versions of smartphone-based fluorescence readers,[21,30–32] which can be adapted for use with this device and even enable fully automated readout by incorporating inexpensive automation approaches also available in the open hardware literature. Indeed, integration with such readout and automation approaches would form part of the future work for further development of this platform to enable deployment and use in resource-poor settings.

An additional comparison can be made here with recent pathogen detection-based assays where with the advance of microfluidic bioassays, especially by integrating PCR, pathogen detection assays have been sensitive enough to detect disease presence,[33,34] even in multiplexed[35] or lateral flow formats,[36,37] which greatly reduces their cost. μMAP is complementary to pathogen-based biomarker detection technology (*e.g.* antigen detection tests such as CAA for schistosomiasis) as antibody Fc modifications still offer a unique disease-state-specific perspective in complement to direct pathogen detection. Though their use for detecting acute disease onset still needs further work, antibody Fc properties offer long-term monitoring and disease state differentiation,[8,9] which often cannot be done based on the abundance of pathogens in the body alone[38] and are where antigen tests often show less ideal performance.

Conclusions

We presented here the μMAP platform: a microscale device and corresponding workflow to perform biomarker discovery targeting antibody Fc features for, but not limited to, endemic infectious diseases. The μMAP chip can perform a total of 1400 assays measuring 100 antibody Fab and Fc features from a sample with low volume (<15 μL). This is currently configured to run 14 samples (vertical channels or columns) × 25 capture antigen spots (at each horizontal/vertical channel intersection) × 4 Fc probes (horizontal channels or rows) but is reconfigurable (*e.g.* for technical/biological repeats) for other applications by the user without any other change in design or operation. While successfully detecting Ab Fc features, including isotype, subclass, *N*-glycosylation and Fc receptor binding, the device exhibits several advantages over existing solutions by using highly multiplexed microarrays, microfluidic channels and cleanroom-free fabrication and pump-free use making it easy to fabricate and use in clinical research labs in resource-poor settings.

We demonstrated the performance of the μMAP platform verifying its specificity, high dynamic range, low LOD and high correlation in comparison with existing methods. Finally, we applied it to clinical patient serum samples to discover biomarkers that differentiate active or current schistosome infection from former or non-patent infections and endemic healthy controls. Beyond this application, the platform is compatible with measuring the same type of interaction measurable by other binding assays without the use of additional sample preparation. Several limitations are related to the principle of the binding-based assays, especially those conducted on 2D surfaces such as the glass slide surface here, including the limited binding capacity per antigen and potential interactions and variants present in serum, such as soluble antigens. Future work includes performing biomarker discoveries for other endemic diseases in the field or in other laboratories, increasing the number of samples that can be tested per device by modifying channel width or substrate size, incorporating pre-printed probes[39] and further improving usability by incorporating feedback from user studies. Additionally, harnessing the ability of the μMAP platform to generate high-dimensional datasets that can be coupled with modern artificial intelligence/machine learning approaches represents an exciting future prospect as well.

Experimental

Materials

Poly-L-lysine slides, phosphate buffer saline (PBS) and deionized (DI) water were purchased from Fisher Scientific (Hampton, NH). Bovine serum albumin (BSA) and human serum for glycoengineering were purchased from Sigma Aldrich (St. Louis, MO). Tween 20 was purchased from VWR (Radnor, PA). Polydimethylsiloxane (PDMS) sheet was purchased from Greene Rubber Company (Woburn, MA). Anti-SARS-CoV-2 spike glycoprotein S1 antibody was purchased from Abcam. GlycoBuffer (1,4), α2-3,6,8,9 neuraminidase A and β1-3,4 galactosidase were purchased from New England Biolabs (Ipswich, MA). Anti-SARS-CoV-2 nucleocapsid-mAb was purchased from Absolute Antibody. All probes targeting human Ig isotypes/subtypes were

purchased from SouthernBiotech (Birmingham, AL). Human Fc gamma RIIA/RIIB were purchased from ACROBiosystems (Newark, Delaware). Streptavidin PE was purchased from Thermo Fisher Scientific (Waltham, MA). *Sambucus nigra* lectin-CY3 and *Ricinus communis* agglutinin I-Rhodamine were purchased from Vector Laboratories (Newark, CA). Schistosome antigens were provided by collaborators. The recombinant antigens rSm25, rSmCD63like, and rSm Calumenin B were identified through size-exclusion chromatography and tandem mass spectrometry, complemented by serum epitope repertoire analysis. Detection of rSm25 and rSmMEG employed an anti-IgG1 antibody, whereas rSm Calumenin B utilized an IgG4 antibody. Clinical SARS-CoV-2 serum samples (healthy/SARS-CoV-2 patient/vaccinated) were purchased from RayBiotech (Peachtree Corners, GA). The vendor obtained serum from donors with informed consent after IRB approval (protocol no. SOP-TF-PH-002 STERLING IRB ID: 8291-BZhang). Details are on file and available from the vendor. Schistosomiasis patient serum samples were obtained from Minas Gerais, Brazil between June 2016 and December 2018 as part of a case-control study. Individuals were tested for *S. mansoni* infection by a stool exam and by serology to SEA. All experiments were performed in accordance with the guidelines of Emory University, and experiments were approved by the ethics committee at Emory University (IRB000857575). Informed consents were obtained from human participants of this study. Details about the cohort and approval are described in earlier studies.[8]

Device preparation

Alignment marks were engraved on slides *via* a CO_2 laser cutter (Universal Laser System, Scottsdale, AZ). Proteins were diluted in 150 mM PBS with various concentrations of glycerol, then printed on slides by a sciFLEXARRAYER S3 microarray printer (Scienion, German). Printed slides were stored at 4 °C until use. PDMS sheets were patterned with the same laser cutter as above. Alignment blocks were created with a Makerbot Method 3D printer (New York, NY).

Antibody *in vitro* glycoengineering

For 0% S serum sample, human serum was incubated with α2-3,6,8,9 neuraminidase A in DI and GlycoBuffer 1 at 37 °C overnight. For 0% G serum sample, 0% S serum was first placed on a hot plate at 65 °C for 10 min. Then it was incubated with β1-3,4 galactosidase in DI and GlycoBuffer 4 at 37 °C overnight to obtain 0% G serum. 100% S and 100% G serum samples were made using the same procedure as for 0% S and 0% G serum samples except neuraminidase/galactosidase was inactivated by incubating on a hot plate at 65 °C for 10 minutes before adding to serum.

Biomarker discovery assay

To perform the biomarker discovery, the μMAP chip was removed from the fridge and blocked with 10% BSA in 0.01%

PBST for 30 minutes. After blocking, the slide was washed in PBST/PBS/DI water then dried with a slide centrifuge. A vertical sample channel PDMS layer and a top cover were attached to the chip using an alignment block (Fig. S1†). Diluted samples were added into the 14 vertical channel layers, then incubated for 1 h. The chip then underwent PDMS removal and went through the same washing/drying process as above. A horizontal probe channel PDMS layer and a top cover were attached to the chip using an alignment block (Fig. S2†). Diluted samples were added into the 4 horizontal channel layers, then incubated for 30 min. The chip then underwent PDMS removal and went through the same washing/drying process as above. The chip was then stored in 4 °C until imaging.

Data acquisition

The chip was restored to room temperature then scanned by an InnoScan microarray scanner (Innopsys, Chicago, IL). Scanned images were processed with ImageJ. Statistical analyses were performed with GraphPad Prism. Limit of detection for monoclonal antibody detection was calculated using the following definition: $LOD = Mean_{blank} + 3 \times StDev_{blank}$ where the blank sample is buffer only ($1 \times PBS$).[40]

Data availability

Further information requests should be directed to and will be fulfilled by the corresponding contact author: Aniruddh Sarkar (aniruddh.sarkar@bme.gatech.edu). All data reported and used in this work will be shared by the corresponding author upon reasonable request.

Author contributions

H. Zhang: conceptualization, methodology, investigation, validation, data curation, formal analysis, visualization, writing – original draft, writing – review & editing. D. Bhakta: conceptualization, methodology, investigation, validation. A. Saha: conceptualization, methodology, investigation. S. Peddireddy: conceptualization, methodology, investigation. S. Bao: methodology, investigation. L. Li: methodology, writing – review & editing. S. Handali: resources, writing – review & editing, W. Secor: resources, writing – review & editing. L. Fraga: resources, writing – review & editing. J. Fairley: resources, writing – review & editing. A. Sarkar: conceptualization, methodology, formal analysis, writing – review & editing, resources, supervision, project administration, funding acquisition. All authors reviewed the manuscript.

Conflicts of interest

All authors declare that they have no competing interests.

Acknowledgements

Notes and references

1 J. P. Townsend, H. B. Hassler, A. D. Lamb, P. Sah, A. A. Nishio, C. Nguyen, A. D. Tew, A. P. Galvani and A. Dornburg, *mBio*, 2023, **14**, e0142623.

2 M. Pai, M. A. Behr, D. Dowdy, K. Dheda, M. Divangahi, C. C. Boehme, A. Ginsberg, S. Swaminathan, M. Spigelman, H. Getahun, D. Menzies and M. Raviglione, *Nat. Rev. Dis. Primers*, 2016, **2**, 16076.

3 A. K. Deol, F. M. Fleming, B. Calvo-Urbano, M. Walker, V. Bucumi, I. Gnandou, E. M. Tukahebwa, S. Jemu, U. J. Mwingira, A. Alkohlani, M. Traore, E. Ruberanziza, S. Toure, M. G. Basanez, M. D. French and J. P. Webster, *N. Engl. J. Med.*, 2019, **381**, 2519–2528.

4 A. A. Justiz Vaillant, Z. Jamal, P. Patel and K. Ramphul, in *StatPearls*, StatPearls Publishing Copyright © 2024, StatPearls Publishing LLC, Treasure Island (FL), 2024.

5 M. D. Swartz, S. M. DeSantis, A. Yaseen, F. A. Brito, M. A. Valerio-Shewmaker, S. E. Messiah, L. G. Leon-Novelo, H. W. Kohl, C. L. Pinzon-Gomez, T. Hao, S. Zhang, Y. Talebi, J. Yoo, J. R. Ross, M. O. Gonzalez, L. Wu, S. H. Kelder, M. Silberman, S. Tuzo, S. J. Pont, J. A. Shuford, D. Lakey and E. Boerwinkle, *J. Infect. Dis.*, 2023, **227**, 193–201.

6 M. Ackerman and F. Nimmerjahn, *Antibody Fc: linking adaptive and innate immunity*, Academic Press, 2013.

7 M. F. Jennewein and G. Alter, *Trends Immunol.*, 2017, **38**, 358–372.

8 A. Saha, T. Chakraborty, J. Rahimikollu, H. Xiao, L. B. P. de Oliveira, T. W. Hand, S. Handali, W. E. Secor, L. A. O. Fraga, J. K. Fairley, J. Das and A. Sarkar, *Sci. Transl. Med.*, 2024, **16**, eadk7832.

9 S. P. Peddireddy, S. A. Rahman, A. R. Cillo, G. M. Vijay, A. Somasundaram, C. J. Workman, W. Bain, B. J. McVerry, B. Methe, J. S. Lee, P. Ray, A. Ray, T. C. Bruno, D. A. A. Vignali, G. D. Kitsios, A. Morris, H. Singh, A. Sarkar and J. Das, *Cell Rep.*, 2022, **39**(13), 111020.

10 M. E. Ackerman, M. Crispin, X. Yu, K. Baruah, A. W. Boesch, D. J. Harvey, A. S. Dugast, E. L. Heizen, A. Ercan, I. Choi, H. Streeck, P. A. Nigrovic, C. Bailey-Kellogg, C. Scanlan and G. Alter, *J. Clin. Invest.*, 2013, **123**, 2183–2192.

11 K. S. Kao, A. Gupta, G. Zong, C. Li, I. Kerschbaumer, S. Borghi, J. M. Achkar, S. Bournazos, L. X. Wang and J. V. Ravetch, *Proc. Natl. Acad. Sci. U. S. A.*, 2022, **119**, e2212658119.

12 L. L. Lu, J. Das, P. S. Grace, S. M. Fortune, B. I. Restrepo and G. Alter, *J. Infect. Dis.*, 2020, **222**, 2093–2102.

13 Y. Rombouts, E. Ewing, L. A. van de Stadt, M. H. Selman, L. A. Trouw, A. M. Deelder, T. W. Huizinga, M. Wuhrer, D. van Schaardenburg, R. E. Toes and H. U. Scherer, *Ann. Rheum. Dis.*, 2015, **74**, 234–241.

14 S. E. de Jong, M. H. Selman, A. A. Adegnika, A. S. Amoah, E. van Riet, Y. C. Kruize, J. G. Raynes, A. Rodriguez, D. Boakye, E. von Mutius, A. C. Knulst, J. Genuneit, P. J. Cooper, C. H. Hokke, M. Wuhrer and M. Yazdanbakhsh, *Sci. Rep.*, 2016, **6**, 28207.

15 F. Dall'Olio, V. Vanhooren, C. C. Chen, P. E. Slagboom, M. Wuhrer and C. Franceschi, *Ageing Res. Rev.*, 2013, **12**, 685–698.

16 E. P. Brown, J. A. Weiner, S. Lin, H. Natarajan, E. Normandin, D. H. Barouch, G. Alter, M. Sarzotti-Kelsoe and M. E. Ackerman, *J. Immunol. Methods*, 2018, **455**, 24–33.

17 E. P. Brown, K. G. Dowell, A. W. Boesch, E. Normandin, A. E. Mahan, T. Chu, D. H. Barouch, C. Bailey-Kellogg, G. Alter and M. E. Ackerman, *J. Immunol. Methods*, 2017, **443**, 33–44.

18 Z. Swank, G. Michielin, H. M. Yip, P. Cohen, D. O. Andrey, N. Vuilleumier, L. Kaiser, I. Eckerle, B. Meyer and S. J. Maerkl, *Proc. Natl. Acad. Sci. U. S. A.*, 2021, **118**(18), e2025289118.

19 D. Kim, G. Biancon, Z. Bai, J. VanOudenhove, Y. Liu, S. Kothari, L. Gowda, J. M. Kwan, N. C. Buitrago-Pocasangre, N. Lele, H. Asashima, M. K. Racke, J. E. Wilson, T. S. Givens, M. M. Tomayko, W. L. Schulz, E. E. Longbrake, D. A. Hafler, S. Halene and R. Fan, *Small Methods*, 2023, **7**, 2300594.

20 H. Torul, Z. Ç. Arslan, T. Tezcan, E. Ç. Kayiş, M. Çalımcı, A. Gumustas, E. Yildirim, H. Külah and U. Tamer, *J. Pharm. Biomed. Anal.*, 2023, **228**, 115313.

21 G. Choi, B. B. Mangadu, Y. K. Light and R. J. Meagher, *Sens. Diagn.*, 2024, **3**, 648–658.

22 G. Liu, H. Huang, Z. Chen, H. Lin, H. Liu, X. Huang and W. Guo, *Integration*, 2022, **82**, 48–66.

23 H.-B. Liu and H.-Q. Gong, *J. Micromech. Microeng.*, 2009, **19**, 037002.

24 E. W. Olle, J. Messamore, M. P. Deogracias, S. D. McClintock, T. D. Anderson and K. J. Johnson, *Exp. Mol. Pathol.*, 2005, **79**, 206–209.

25 M. Cohen, M. Elkabets, M. Perlmutter, A. Porgador, E. Voronov, R. N. Apte and R. G. Lichtenstein, *J. Immunol.*, 2010, **185**, 5869–5878.

26 W. K. You, I. Kasman, D. D. Hu-Lowe and D. M. McDonald, *Am. J. Pathol.*, 2010, **176**, 1927–1940.

27 T. Petrović, A. Vijay, F. Vučković, I. Trbojević-Akmačić, B. J. Ollivere, D. Marjanović, T. Bego, B. Prnjavorac, L. Đerek, A. Markotić, I. Lukšić, I. Jurin, A. M. Valdes, I. Hadžibegović and G. Lauc, *EBioMedicine*, 2022, **81**, 104101.
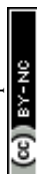
28 E. Ponzo, A. Midiri, A. Manno, M. Pastorello, C. Biondo and G. Mancuso, *Eur. J. Microbiol. Immunol.*, 2024, **14**, 86–96.

29 H. W. Jiang, Y. Li, H. N. Zhang, W. Wang, X. Yang, H. Qi, H. Li, D. Men, J. Zhou and S. C. Tao, *Nat. Commun.*, 2020, **11**, 3581.

30 J. F. Bergua, R. Álvarez-Diduk, A. Idili, C. Parolo, M. Maymó, L. Hu and A. Merkoçi, *Anal. Chem.*, 2022, **94**, 1271–1285.

31 A. Prasad, S. M. A. Hasan, S. Grouchy and M. R. Gartia, *Analyst*, 2019, **144**, 197–205.

32 G.-R. Han, A. Goncharov, M. Eryilmaz, H.-A. Joung, R. Ghosh, G. Yim, N. Chang, M. Kim, K. Ngo, M. Veszpremi, K. Liao, O. B. Garner, D. Di Carlo and A. Ozcan, *ACS Nano*, 2024, **18**, 27933–27948.

33 Q. Liu, X. Jin, J. Cheng, H. Zhou, Y. Zhang and Y. Dai, *Mol. Med. Rep.*, 2023, **27**, 104.

34 P. Zhang, J. Hu, J. S. Park, K. Hsieh, L. Chen, A. Mao and T.-H. Wang, *Anal. Chem.*, 2022, **94**, 12481–12489.

35 Y. Zhao, C. M. O'Keefe, J. Hu, C. M. Allan, W. Cui, H. Lei, A. Chiu, K. Hsieh, S. C. Joyce, J. G. Herman, T. R. Pisanic and T.-H. Wang, *Sci. Adv.*, 2024, **10**, eadp1704.

36 W. Pengcheng, S. Jiaren, S. Caixia, Z. Wanchao, D. Jianjun and J. Yanmin, *TrAC, Trends Anal. Chem.*, 2023, **166**, 117203.

37 K. Hallerbach, K. Khederlou, L. Wentland, L. Senten, S. Brentano, B. Keefe and E. Fu, *Micromachines*, 2023, **14**, 1936.

38 O. Ally, B. N. Kanoi, L. Ochola, S. G. Nyanjom, C. Shiluli, G. Misinzo and J. Gitaka, *PLoS Neglected Trop. Dis.*, 2024, **18**, e0012282.

39 D. S. Kinnamon, J. T. Heggestad, J. Liu, T. Nguyen, V. Ly, A. M. Hucknall, C. M. Fontes, R. J. Britton, J.-P. Cai, J. F.-W. Chan, K.-Y. Yuen, T. Le and A. Chilkoti, *ACS Sens.*, 2023, **8**, 2228–2236.

40 M. Cavaiuolo, S. Paramithiotis, E. H. Drosinos and A. Ferrante, *Anal. Methods*, 2013, **5**, 4622–4627.